Simulation of sodium diborate glass containing lead and cadmium oxides for radiation shielding applications

M. M. Damoom[a,b], A. M. Alhawsawi[a,b], E. Banoqitah[a,b], E. B. Moustafa[c], O. H. Sallam[d], A. H. Hammad[e,*]
[a]*Nuclear Engineering Department, Faculty of Engineering, King Abdulaziz University, P.O. Box 80204, 21589 Jeddah, Saudi Arabia*
[b]*Center for Training & Radiation Prevention, King Abdulaziz University, P.O. Box 80204, Jeddah, 21589, Saudi Arabia*
[c]*Mechanical Engineering Department, Faculty of Engineering, King Abdulaziz University, P.O. Box 80204, 21589 Jeddah, Saudi Arabia*
[d]*Nuclear and Radiological Safety Research Center (NRSRC), Atomic Energy Authority, Cairo, Egypt*
[e]*Center of Nanotechnology, King Abdulaziz University, Jeddah 21589, Saudi Arabia*

Sodium diborate glasses containing cadmium and lead oxides were fabricated by the melt annealing technique. Lead oxide was introduced at the expense of cadmium oxide to enhance its elastic and shielding properties. The density of the lead-free glass increased from 2.137 g/cm^3 to 3.330 g/cm^3 after replacing cadmium oxide with lead oxide. The density values were used to investigate the elastic properties of glass using the Makishima-Mackenzie model. In addition, the Phy-X/PSD code was used to simulate the shielding properties of such glasses at different photon energies ranging from 0.005 to 15 MeV.

(Received Feburary 7, 2024; Accepted May 8, 2024)

Keywords: Borate, Lead ions, Density, Elastic properties, Phy-x/PSD code, Shielding properties

1. Introduction

Many noteworthy physical and chemical properties are associated with glass, such as its high density, remarkable light transparency, remarkable corrosion resistance, and compositional versatility. Furthermore, glass can be produced using a range of techniques. The addition of heavy metal oxides, in particular lead oxide (PbO), to oxide glass formers produces glass that is stronger and has remarkable optical, structural, physical, and shielding properties [1-4]. In contrast to other oxide glasses like silicate (SiO_2) and phosphate (P_2O_5), borate (B_2O_3) is thought to be a feasible glass former when it comes to radiation shielding design.

Lead is a noteworthy material in optical fields and radiation shielding applications due to its high density (11.34 g/cm^3) [5, 6]. Lead-containing glasses have tunable mechanical, chemical, and optical properties as well as good neutron, gamma, and X-ray attenuation, according to Abouhaswa et al. [7]. Several studies have been conducted to verify the shielding effectiveness of lead glasses, in which the structural elements of the glasses have been modified by adding various transition metal oxides to suit particular application scenarios. Kaur and Singh [8] examined the shielding properties of borate glass that contained lead and aluminum oxides. Similar to this, a study on lead borate glass was carried out by Abouhaswa et al. [7], who added La as an additive for shielding. Furthermore, the shielding qualities of zinc borate glass containing lead oxide were investigated by Ghamdi et al. [9].

The current study looked into the sodium borate cadmium glass system with varying lead oxide concentrations at the expense of cadmium oxide. The glass density was experimentally

* Corresponding author: ahhhassan@kau.edu.sa
https://doi.org/10.15251/JOR.2024.203.285

determined to derive the elastic properties via the Makishima-Mackenzie model. For every glass sample, the Phy-X/PSD simulation was used to evaluate radiation shielding parameters. The mass and linear attenuation (*MAC* and *LAC*) values were used to calculate and interpret the different shielding parameters in terms of the PbO content.

2. Experimental

The formula for the glass nominal used in this study is $20Na_2O–40B_2O_3–(40\text{-}x)CdO–xPbO$, where x = 0, 10, 20, 30, and 40 mol%. Borax salt is the source of Na_2O and B_2O_3, while PbO is derived from Pb_3O_4, and CdO has been purchased in its original form. Every chemical is 99%. After the batch was weighed, it was melted for two hours at 1250 °C in an electrical furnace. Samples that were melted were poured into a specially prepared graphite mold to form the glass sample. The glass density was ascertained using Archimedes' principle, wherein the glass was measured for weight suspended in air (W_A) and immersed in xylene (W_L).

3. Methodology and computation methods

3.1. Density and molar volume

The measured density (D_{exp}) was carried out using the Archimedes principle. This calculation was performed using the following equation [10]:

$$D_{exp}(g/cm^3) = \frac{W_A}{W_A - W_l} \times 0.863 \tag{1}$$

The molar volume (V_m) of the glass sample was derived by employing the given equation, which involved the measured glass density (D_{exp}) and the average molecular weight of the sample (M_{wt}) [11].

$$V_m\ (cm^3/mol) = M_{wt}/D_{exp} \tag{2}$$

3.2. The elastic parameters

The mechanical parameters, namely Young's modulus (E), bulk modulus (K), shear modulus (G), Poisson's ratio (s), and the hardness value (H_v), can be evaluated through the utilization of the packing ratio (V_p) and the unit volume of dissociation energy (G_i), as expressed by the following equations [12-19]:

$$V_p = D_{exp} \times \frac{\sum V_i x_i}{\sum M_i x_i} \tag{3}$$

where the packing density parameter (V_i) is expressed in cubic centimeters per mole. The ratio of the metal oxide in mole fraction (x_i) is determined, and the molecular weight of the element (M_i) is denoted. The product of the molecular weight (M_i) and the mole fraction (x_i) is represented as $\sum M_i x_i$, which corresponds to the molecular weight of the glass (M_{wt}).

$$E = 8.36\, V_P \sum G_i x_i \tag{4}$$

$$K = 10 V_P^2 \sum G_i x_i \tag{5}$$

$$G = \frac{30 V_P^2}{10.2 V_P - 1} \sum G_i x_i \tag{6}$$

$$\sigma = 0.5 - (7.2 V_P)^{-1} \tag{7}$$

$$H_v = G/6.78 \tag{8}$$

3.3. Shielding parameters simulation

Photon Shielding and Dosimetry (PSD) is a web-based software application that can be accessed at https://phy-x.net/PSD [20]. PSD facilitates the calculation of various radiation parameters. The parameters covered in this study consist of linear and mass attenuation coefficients (*LAC*, *MAC*), half and tenth value layers (*HVL*, *TVL*), mean free path (*MFP*), and effective atomic number (Z_{eff}). The software has the capability to produce data pertaining to shielding parameters within the energy range of 1 keV to 100 GeV. The subsequent equations are employed for the computation of the radiation parameters [21-24]:

$$LAC\ (cm^{-1}) = MAC \times D \tag{9}$$

$$HVL\ (cm) = 0.693/LAC \tag{10}$$

$$TVL\ (cm) = 2.303/LAC \tag{11}$$

$$MFP\ (cm) = 1/LAC \tag{12}$$

$$Z_{eff} = \frac{\sigma_a}{\sigma_e} = \frac{\frac{1}{N_A}\sum f_i A_i (MAC)_i}{\frac{1}{N_A}\sum \frac{f_i A_i (MAC)_i}{Z_i}} \tag{13}$$

In the given equation, N_A denotes Avogadro's number, σ_a and σ_e are the atomic and electronic cross sections, A_i and Z_i symbolize atomic weight and number of an element i, and f_i signifies the fraction of element i.

3. Results and discussion

3.1. The glass density and the elastic parameters

The density (D_{exp}) of a sodium borate glass with a 40% cadmium oxide composition was determined to be 2.137 g/cm^3. Subsequently, when the cadmium oxide (CdO) replaced lead oxide (PbO), the D_{exp} raised to 3.33 g/cm^3. The relationship between the D_{exp} and the PbO content is illustrated in Fig. 1. The rise in D_{exp} values may be attributed to the replacement of low-density CdO (6.95 g/cm^3) with high-density PbO (9.53 g/cm^3). The density values of these glasses exhibit a lower magnitude compared to the findings reported by Yasser B. Saddeek [25]. The measurements indicated a density of 2.377 g/cm^3 for sodium diborate glass and 4.060 g/cm^3 for the 20 Na_2O–40 B_2O_3–40 PbO glass composition [25].

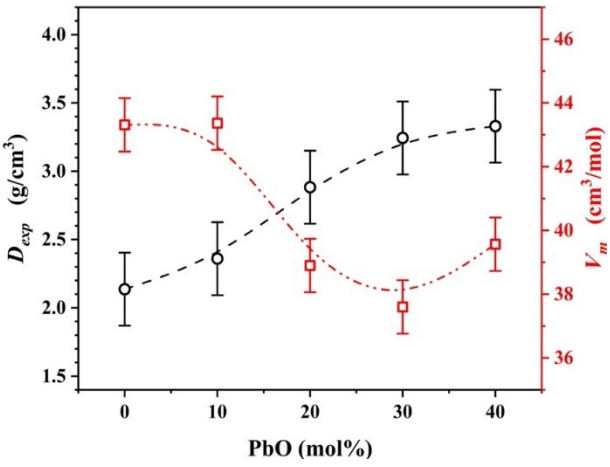

Fig. 1. The correlation between the glass density and molar volume and the glass composition.

In contrast, it was observed that the molar volume of the glass exhibited a decrease as the PbO content increased. Specifically, the molar volume (V_m) decreased from 43.311 cm^3/mol at 0 PbO to 39.565 cm^3/mol at 40% PbO. This decrease suggests that structural modifications occur in these glasses as a result of the substitution of CdO with PbO and alterations in the concentration of glass network constituents, such as BO_3 and BO_4 structural units. Table 1 presents the data relating to the molecular weight (M_{wt}), D_{exp}, and V_m for various compositions of sodium borate glass.

Table 1. The values of some physical and mechanical parameters, such as average molecular weight (M_{wt}), glass density (D_{exp}), molar volume (V_m), Young's modulus (E), bulk modulus (K), shear modulus (G), Poisson's ratio (σ), and the hardness value (H_v).

	0 PbO	**10 PbO**	**20 PbO**	**30 PbO**	**40 PbO**
M_{wt} **(g)**	92.534	102.340	112.143	121.950	131.752
D_{exp} **(g/cm^3)**	2.137	2.360	2.883	3.244	3.330
V_m **(cm^3/mol)**	43.311	43.364	38.897	37.597	39.565
***E* (GPa)**	53.720	54.153	60.324	61.982	58.154
***K* (GPa)**	33.678	35.201	44.963	48.910	44.894
G (GPa)	21.763	21.773	23.631	24.050	22.686
σ	0.235	0.244	0.277	0.289	0.282
H_v **(GPa)**	3.210	3.211	3.485	3.546	3.346

The elastic properties of the current glasses are contingent upon their composition and structure. As illustrated in Fig. 2, the elastic parameters exhibited a positive trend with increasing PbO content up to 30%, followed by a slight decrease at 40% PbO. Specifically, the *E* increased from 53.719 GPa to 58.154 GPa as the PbO rose from 0 to 40 mol%. Similarly, the bulk modulus and shear modulus increased from 33.678 GPa to 44.394 GPa and 21.763 GPa to 22.687 GPa, respectively. Additionally, the Poisson's ratio and hardness values increased from 0.235 to 0.282 and from 3.210 GPa to 3.346 GPa, respectively, with an increase in PbO content. Notably, the glass sample containing 30 mol% PbO exhibited the highest elastic parameter values, as shown in Table 1. The elastic properties of the present glass samples were found to be superior to those documented in the literature for Bi_2O_3-PbO-B_2O_3:SnO_2 glass [26]. Specifically, the Young's modulus (*E*) demonstrated a notable improvement, increasing by a factor of 1.92. Additionally, the bulk modulus (*K*) exhibited a substantial increase of 2.38 times, while the shear modulus (*G*) experienced a significant enhancement of 1.85 times [26]. Furthermore, the present dataset exhibits elevated values in comparison to those documented in the CuO–CaO–B_2O_3–PbO glass [27]. Nevertheless, the aforementioned parameters exhibit lower values compared to the ones documented in CdO–PbO–ZnO–B_2O_3–SiO_2 glass [28].

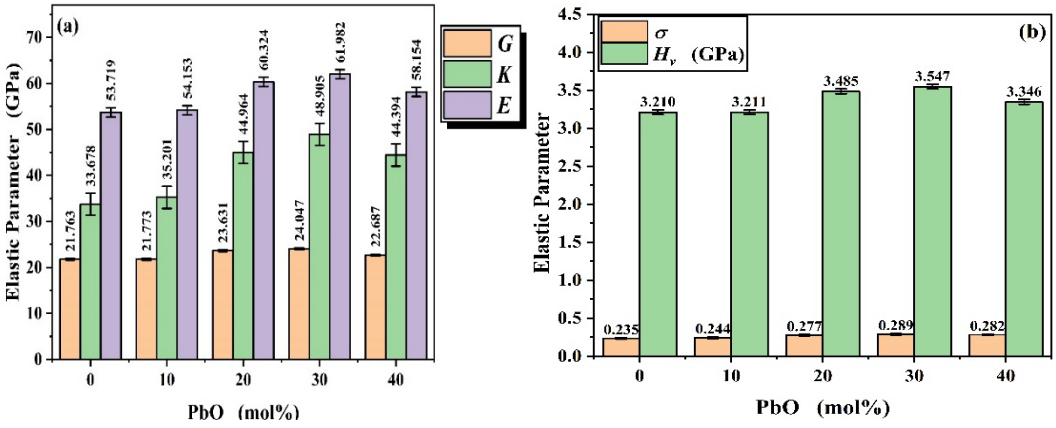

Fig. 2. Dependence of the elastic parameters on the glass composition: (a) Young's (E), bulk (K), and shear (G) moduli. (b) Poisson's ratio (σ) and the hardness value (H_v).

3.2. The shielding characteristics

3.2.1. The Mass attenuation coefficient

The *MAC* can be derived by utilizing the values of the *LAC* as specified in equation (9). The *LAC* values corresponding to various types of glasses are provided in Table 2. Fig. 3 depicts the relationship between the *MAC* and the incident photon energies across various glass compositions. The dependence of *MAC* curves is contingent upon the specific photon energy regime, namely the photoelectric (PE; 0.005 MeV–0.1 MeV), Compton scattering (CS; 0.1 MeV–12 MeV), and pair production (PP; >12 MeV) regimes [5, 18, 29-34]. A notable pattern observed in the behavior of *MAC* (mass attenuation coefficient) is a significant decrease in *MAC* values within the PE (photoelectric effect) region. This decrease is found to be correlated with the photon energy ($E_n^{-3.5}$). The observed change in the surface area of the 0 pbO glass sample was significant, decreasing from 264.354 cm^2/g to 0.825 cm^2/g, as the photon energy was raised from 0.00589 MeV to 0.1 MeV. Upon further increasing the photon energy to 10 MeV, the mass attenuation coefficient (*MAC*) exhibited a decrease to 0.029 cm^2/g (the partial cross section is inversely proportion to the photon energy). Subsequently, in the pair production (PP) region at 15 MeV, the *MAC* experienced a slight increase to 0.03 cm^2/g (the partial cross section is related to the log (E_n).

Table 2. Some values of the linear attenuation coefficient (LAC) of Na_2O–B_2O_3–CdO–PbO glasses at different photon energies.

Photon Energy (MeV)	***LAC* (cm^{-1})**				
	0 PbO	**10 PbO**	**20 PbO**	**30 PbO**	**40 pbO**
0.00589	564.9248	670.8300	866.0745	1019.0842	1086.8778
0.01381	57.6619	111.7811	184.7214	253.5120	300.5727
0.025	11.6779	32.5815	59.5250	85.6645	104.4097
0.05	10.4985	11.8415	14.7027	16.7785	17.4617
0.08	3.0683	3.5226	4.4348	5.1174	5.3737
0.1	1.7655	4.0734	7.1035	10.0089	12.0525
0.3	0.2786	0.4340	0.6567	0.8587	0.9871
0.5	0.1899	0.2442	0.3328	0.4072	0.4468
0.723	0.1536	0.1832	0.2374	0.2800	0.2987
1	0.1289	0.1481	0.1867	0.2156	0.2261
1.173	0.1183	0.1344	0.1679	0.1924	0.2006
1.275	0.1132	0.1280	0.1594	0.1822	0.1895
1.333	0.1106	0.1249	0.1553	0.1773	0.1842
1.408	0.1076	0.1212	0.1505	0.1717	0.1783
1.5	0.1042	0.1173	0.1455	0.1658	0.1721
2	0.0908	0.1024	0.1271	0.1449	0.1505
2.506	0.0825	0.0935	0.1167	0.1336	0.1391
3	0.0771	0.0879	0.1102	0.1267	0.1325
4	0.0703	0.0814	0.1031	0.1196	0.1259
5	0.0667	0.0781	0.1000	0.1168	0.1237
10	0.0627	0.0768	0.1013	0.1211	0.1307
15	0.0645	0.0809	0.1085	0.1312	0.1428

The incorporation of lead oxide (PbO) into the glass structure results in an elevation of the *MAC* values. At a photon energy of 0.00589 MeV, the *MAC* exhibited a 7.5 timed increase when the PbO ratio was 10%. Furthermore, the *MAC* increased to 23.5 times its initial value when the glass was devoid of CdO content, with a PbO ratio of 40%. Similar patterns of behavior were observed across various energy ranges. Moreover, the spectra of *MAC* exhibit certain edges that suggest the presence of absorption edges corresponding to the following:

i- The L_3 absorption edge of lead (Pb) was detected at 0.01304 MeV.
ii- The L_1 absorption edge of lead (Pb) was detected at 0.01586 MeV.
iii- The *K* absorption edge of Cadmium (Cd) was observed at 0.02671 MeV.
iv- The *K* absorption edge of lead (Pb) was determined at 0.088 MeV.

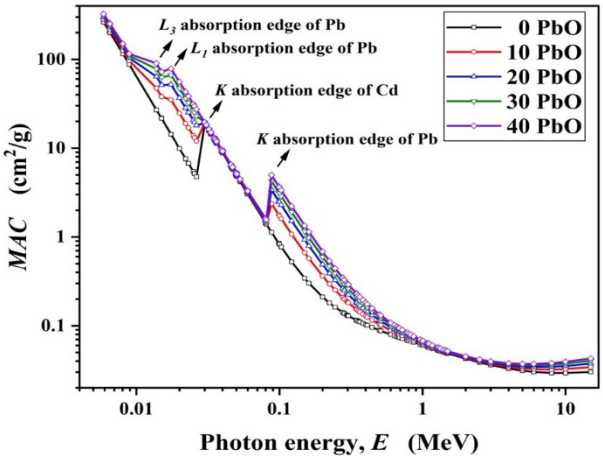

Fig. 3. The mass attenuation coefficient (MAC) at different photon energies for cadmium sodium diborate glass containing lead oxide.

3.2.2. The half and tenth value layers

HVL and *TV*L are utilized as metrics to assess a material's behavior to attenuate incident photon energies 50% and 10% of their original values, respectively. Fig. 4 illustrates the change in the *HVL* and *TVL* across glasses within distinct photon energy ranges.

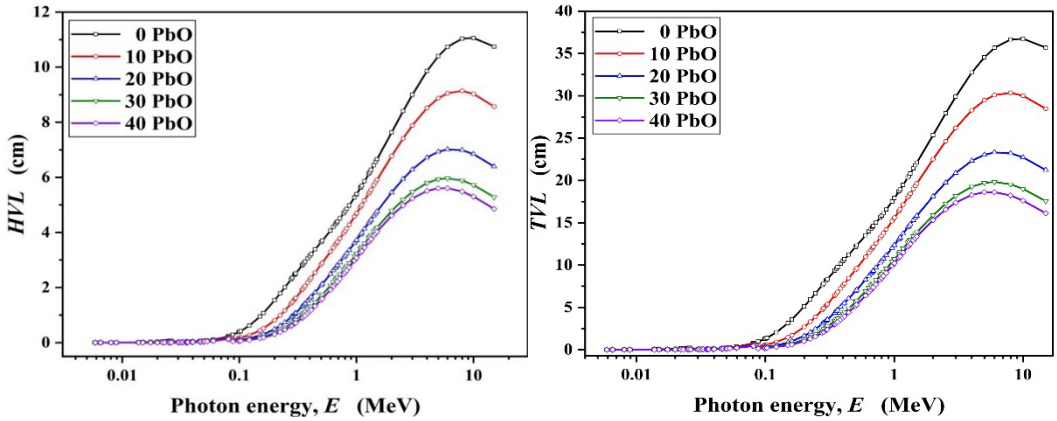

Fig. 4. The half and tenth value layers (HVL and TVL) at different photon energies for different glass compositions.

In the context of the PE region, it is observed that both the *HVL* and the *TVL* exhibit reduced magnitudes. Consequently, it can be inferred that any of the presently available glasses are capable of effectively attenuating radiation intensity to a minimum level or within the safety threshold. To illustrate, the *HVL* for the free PbO glass (0 PbO) was measured to be 0.0123 mm at an energy of 0.00589 MeV, and 4 cm at an energy of 0.1 MeV. Within the context of the CS regime, it is observed that the *HVL* exhibits an upward trend as the energy of photons increases. Specifically, at an energy level of 10 MeV, the *HVL* reaches a value of 11 cm. However, a slight reduction is observed at 15 MeV, resulting in an *HVL* of 10.75 cm. This decrease could be related to the pair production (PP) process. The presence of PbO resulted in a reduction in *HVL* values, with a reduction of 48% when compared to the free PbO sample at 0.00589 MeV, 0.6 mm at 0.1 MeV, and 5.3 cm at 10 MeV for 40% PbO. The similar behavior is observed for the *TVL* behavior, as the *TVL* can be calculated directly from the *HVL*.

3.2.3. The mean free path and the effective atomic number

MFP pertains to the average distance traversed by atoms, molecules, or photons, prior to undergoing substantial alterations in its trajectory, energy, or other characteristics.

Shielding technology typically favors a lower value of the *MFP*. As depicted in Fig. 5, the *MFP* was observed to be approximately 0.02 ml within the lower range of photon energies, particularly in the photoelectric (PE) region. This measurement was obtained for the 0 PbO sample within the energy from 0.00589 MeV to 0.00654 MeV. Subsequently, the *MFP* increased to 5.7 mm at energy of 0.1 MeV. The *MFP* within the CS region exhibited a significant increase, reaching 7.76 cm at 1 MeV and 16 cm at 10 MeV. Additionally, the inclusion of lead oxide (PbO) in the network made a decrease in the *MFP* values within the PE and CS regions. Hence, the inclusion of PbO enhances the shielding characteristic observed in these materials.

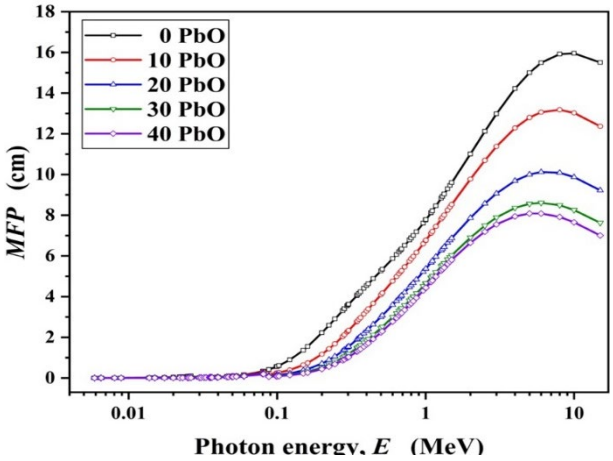

Fig. 5. The dependence of the mean free path (MFP) on the photon energies for the studied glasses.

The behavior of the glasses in terms of the Z_{eff} is illustrated in Fig. 6. The observed samples exhibit a range of Z_{eff} values at lower photon energies, spanning from 0.00589 MeV to 0.1 MeV. In the region beyond the photoelectric (PE) effect, there was a significant decrease in the effective nuclear charge (Z_{eff}) from 32.075 to 18.467, corresponding to an increase in energy from 0.1 MeV to 15 MeV for the sample of lead oxide (PbO). Nevertheless, the introduction of PbO into the glass led to an increase in the Z_{eff} values at specific energy levels. Specifically, the Z_{eff} values increased from 37.3 to 62.82 at an energy of 0.00589 MeV, from 32.075 to 71.51 at 0.1 MeV, from 12.65 to 19.47 at 1 MeV, and from 18.47 to 33.346 at 15 MeV, as the PbO content varied from 0 to 40%. Therefore, the Z_{eff} values are impacted by the lead oxide contents.

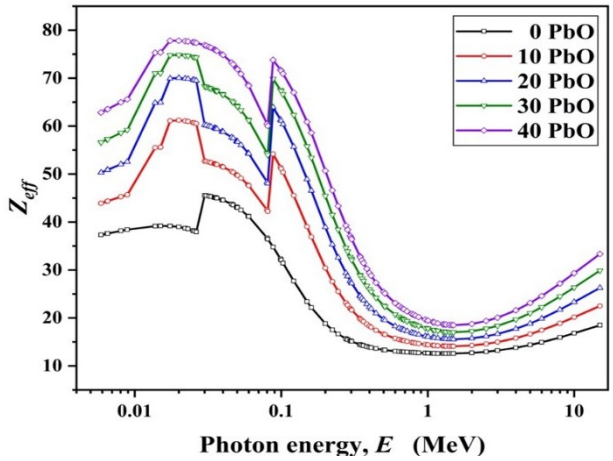

Fig. 6. The effective atomic number (Z_{eff}) of the current glasses at different energies.

4. Conclusion

The present study involved the successful preparation and investigation of glasses containing cadmium sodium diborate, with a cadmium content of 40 mol%. The investigation encompassed an analysis of the glasses' density, elastic, and shielding properties. The incorporation of PbO into the host network was achieved by substituting the CdO component. The incorporation of PbO into the glass network resulted in an enhancement of these parameters, leading to increased hardness values and Poisson's ratios. The Phy-X PSD software was utilized to predict and simulate the shielding parameters. These glasses exhibit a shielding effect against photons, X-rays, and gamma rays. The glass composition containing 40 mol% PbO exhibits a relatively high effective atomic number of 71.51 at an energy level of 0.1 MeV.

Acknowledgements

This research work was funded by Institutional Fund Projects under grant no. (IFPIP: 1689-135-1443). The authors gratefully acknowledge technical and financial support provided by the Ministry of Education and King Abdulaziz University, DSR, Jeddah, Saudi Arabia.

References

[1] P. Kaur, D. Singh, T. Singh, Nuclear Engineering and Design 307, 364 (2016); https://doi.org/10.1016/j.nucengdes.2016.07.029

[2] U. Iliyasu, M. S. Mohd Sanusi, N. E. Ahmad, Radiation Physics and Chemistry 209, 111007 (2023); https://doi.org/10.1016/j.radphyschem.2023.111007

[3] M. Kamislioglu, Results Phys 22, 103844 (2021); https://doi.org/10.1016/j.rinp.2021.103844

[4] M. I. Sayyed, K. M. Kaky, D. K. Gaikwad, O. Agar, U. P. Gawai, S. O. Baki, J Non Cryst Solids 507, 30 (2019); https://doi.org/10.1016/j.jnoncrysol.2018.12.010

[5] A. M. A. Mostafa, S. A. M. Issa, M. I. Sayyed, J Alloys Compd 708, 294 (2017); https://doi.org/10.1016/j.jallcom.2017.02.303

[6] S. A. M. Issa, H. O. Tekin, T. T. Erguzel, G. Susoy, Appl Phys A Mater Sci Process 125, 1 (2019); https://doi.org/10.1007/s00339-019-2941-x

[7] A. S. Abouhaswa, R. El-Mallawany, Y. S. Rammah, Radiation Physics and Chemistry 177, 109085 (2020); https://doi.org/10.1016/j.radphyschem.2020.109085

[8] S. Kaur, K. J. Singh, Ann Nucl Energy 63, 350 (2014); https://doi.org/10.1016/j.anucene.2013.08.012

[9] H. Al-Ghamdi, A. H. Almuqrin, M. S. I. Koubisy, K. A. Mahmoud, M. I. Sayyed, M. A. Darwish, A. M. A. Henaish, Optik (Stuttg) 246, 167765 (2021); https://doi.org/10.1016/j.ijleo.2021.167765

[10] A. M. Abdelghany, A. H. Hammad, Spectrochim Acta A Mol Biomol Spectrosc 137, 39 (2015); https://doi.org/10.1016/j.saa.2014.08.012

[11] H. A. Elbatal, Z. S. Mandouh, H. A. Zayed, S. Y. Marzouk, G. M. Elkomy, A. Hosny, J Non Cryst Solids 358, 1806 (2012); https://doi.org/10.1016/j.jnoncrysol.2012.05.026

[12] S. Inaba, S. Fujino, Journal of the American Ceramic Society 93, 217 (2010); https://doi.org/10.1111/j.1551-2916.2009.03363.x

[13] S. Toyoda, S. Fujino, K. Morinaga, J Non Cryst Solids 321, 169 (2003); https://doi.org/10.1016/S0022-3093(03)00174-1

[14] R. D. Shannon, C. T. Prewitt, Acta Crystallographica Section B 26, 1046 (1970); https://doi.org/10.1107/S0567740870003576

[15] R. D. Shannon, C. T. Prewitt, Acta Crystallographica Section B 25, 925 (1969); https://doi.org/10.1107/S0567740869003220

[16] A. Makishima, J. D. Mackenzie, J Non Cryst Solids 12, 35 (1973); https://doi.org/10.1016/0022-3093(73)90053-7

[17] A. Makishima, J. D. Mackenzie, J Non Cryst Solids 17, 147 (1975); https://doi.org/10.1016/0022-3093(75)90047-2

[18] J. Singh, V. Kumar, Y. K. Vermani, M. S. Al-Buriahi, J. S. Alzahrani, T. Singh, Ceram Int 47, 21730 (2021); https://doi.org/10.1016/j.ceramint.2021.04.188

[19] X. Jiang, J. Zhao, X. Jiang, Comput Mater Sci 50, 2287 (2011); https://doi.org/10.1016/j.commatsci.2011.01.043

[20] E. Şakar, Ö. F. Özpolat, B. Alım, M. I. Sayyed, M. Kurudirek, Radiation Physics and Chemistry 166, 108496 (2020); https://doi.org/10.1016/j.radphyschem.2019.108496

[21] H. O. Tekin, O. Kilicoglu, E. Kavaz, E. E. Altunsoy, M. Almatari, O. Agar, M. I. Sayyed, Results Phys 12, 1797 (2019); https://doi.org/10.1016/j.rinp.2019.01.060

[22] J. H. Hubbell, X-Ray Spectrometry 28, 215 (1999); https://doi.org/10.1002/(SICI)1097-4539(199907/08)28:4<215::AID-XRS336>3.0.CO;2-5

[23] J. H. Hubbell, Phys Med Biol 44, (1999); https://doi.org/10.1088/0031-9155/44/1/001

[24] A. Un, T. Caner, Ann Nucl Energy 65, 158 (2014); https://doi.org/10.1016/j.anucene.2013.10.041

[25] Y. B. Saddeek, J Alloys Compd 467, 14 (2009); https://doi.org/10.1016/j.jallcom.2007.11.126

[26] M. A. Alothman, R. Kurtulus, I. O. Olarinoye, T. Kavas, C. Mutuwong, M. S. Al-Buriahi, Optik (Stuttg) 248, 168047 (2021); https://doi.org/10.1016/j.ijleo.2021.168047

[27] M. Ezzeldin, L. M. Al-Harbi, M. S. Sadeq, A. E. razek Mahmoud, M. A. Muhammad, H. A. Ahmed, Ceram Int 49, 19160 (2023); https://doi.org/10.1016/j.ceramint.2023.03.042

[28] Y. Al-Hadeethi, M. I. Sayyed, B. M. Raffah, A. Kumar, Optik (Stuttg) 257, 168853 (2022); https://doi.org/10.1016/j.ijleo.2022.168853

[29] M. I. Sayyed, S. Hashim, K. G. Mahmoud, A. Kumar, Optik (Stuttg) 274, (2023); https://doi.org/10.1016/j.ijleo.2023.170532

[30] A. B. Chilton, J. K. Shultis, R. E. Faw, Principles of Radiation Shielding, First Edition, Prentice Hall, New Jercy, 1984.

[31] S. A. Bassam, K. A. Naseer, V. K. Keerthana, P. Evangelin Teresa, C. S. Suchand Sangeeth, K. A. Mahmoud, M. I. Sayyed, M. S. Alqahtani, E. El Shiekh, M. U. Khandaker, Radiation Physics and Chemistry 206, 110798 (2023); https://doi.org/10.1016/j.radphyschem.2023.110798

[32] N. K. Libeesh, K. A. Naseer, S. Arivazhagan, K. A. Mahmoud, M. I. Sayyed, M. S. Alqahtani, E. S. Yousef, The European Physical Journal Plus 2022 137:2 137, 1 (2022); https://doi.org/10.1140/epjp/s13360-022-02473-5

[33] N. K. Libeesh, K. A. Naseer, K. A. Mahmoud, M. I. Sayyed, S. Arivazhagan, M. S. Alqahtani, E. S. Yousef, M. U. Khandaker, Radiation Physics and Chemistry 193, 110004 (2022); https://doi.org/10.1016/j.radphyschem.2022.110004

[34] S. Arivazhagan, K. A. Naseer, K. A. Mahmoud, K. V. Arun Kumar, N. K. Libeesh, M. I. Sayyed, M. S. Alqahtani, E. S. Yousef, M. U. Khandaker, Radiation Physics and Chemistry 196, 110108 (2022); https://doi.org/10.1016/j.radphyschem.2022.110108